JACS
JOURNAL OF THE AMERICAN CHEMICAL SOCIETY
pubs.acs.org/JACS
Article

Design Rules, Accurate Enthalpy Prediction, and Synthesis of Stoichiometric Eu^{3+} Quantum Memory Candidates

Zachary W. Riedel and Daniel P. Shoemaker*

Cite This: J. Am. Chem. Soc. 2024, 146, 2113−2121
Read Online
ACCESS | Metrics & More | Article Recommendations | Supporting Information

ABSTRACT: Stoichiometric Eu^{3+} compounds have recently shown promise for building dense, optically addressable quantum memory as the cations' long nuclear spin coherence times and shielded 4f electron optical transitions provide reliable memory platforms. Implementing such a system, though, requires ultranarrow, inhomogeneous linewidth compounds. Finding this rare linewidth behavior within a wide range of potential chemical spaces remains difficult, and while exploratory synthesis is often guided by density functional theory (DFT) calculations, lanthanides' 4f electrons pose unique challenges for stability predictions. Here, we report DFT procedures that reliably reproduce known phase diagrams and correctly predict two experimentally realized quantum memory candidates. We are the first to synthesize the double perovskite halide Cs_2NaEuF_6. It is an air-stable compound with a calculated band gap of 5.0 eV that surrounds Eu^{3+} with mononuclidic elements, which are desirable for avoiding inhomogeneous linewidth broadening. We also analyze computational database entries to identify phosphates and iodates as the next generation of chemical spaces for stoichiometric quantum memory system studies. This work identifies new candidate platforms for exploring chemical effects on quantum memory candidates' inhomogeneous linewidth while also providing a framework for screening Eu^{3+} compound stability with DFT.

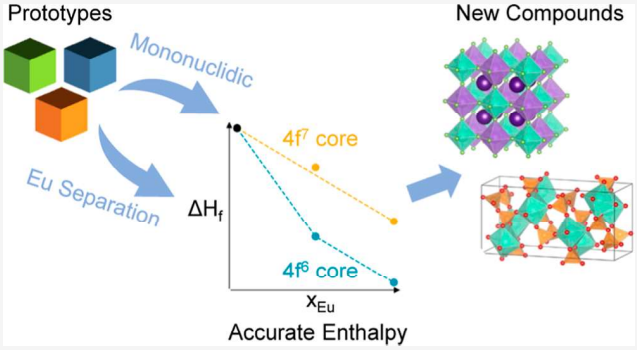

INTRODUCTION

Rare-earth cations have up to 6 h hyperfine energy level coherence times and several millisecond optical coherence times because of 4f-4f orbital optical transitions well-shielded by filled 5s and 5p orbitals.[1−4] The long-lived states allow for a faithful transfer between optical and spin qubits. Building rare-earth qubits typically involves low dopant concentrations to improve coherence times, but along with low optical density comes site inhomogeneity and reduced efficiency. However, stoichiometric rare-earth materials with drastically higher rare-earth concentrations and improved site homogeneity can reduce inhomogeneous linewidths to the point that transitions involving hyperfine energy levels separated by only ∼70−140 MHz are resolved.[5] Promisingly, $EuCl_3{\cdot}6H_2O$ has demonstrated an ultranarrow $^5D_0 \rightarrow {}^7F_0$ transition linewidth paired with a near-millisecond coherence time,[6−9] but its environmental instability and needed isotopic enrichment prompt searches for additional candidates.

A desirable candidate would be air-stable, have a large europium cation separation to limit unintended interactions, consist of mononuclidic elements, and have a polar europium site symmetry to allow the observation of the narrow $^5D_0 \rightarrow {}^7F_0$ transition. These conditions, along with europium's tendency to be divalent, severely limit the known viable materials that may achieve the desired narrow inhomogeneous linewidth. On the other hand, the chemical similarity of lanthanide elements makes them ideally suited for using known structures as prototypes for building unrealized Eu^{3+} compounds. With prototype structures from material databases, we quickly increase our potential candidate list but with no indication of chemical stability.

Density functional theory (DFT) calculations may therefore guide the synthesis efforts of the proposed candidates. Still, care must be taken with DFT calculations to handle the high-energy but spatially shielded 4f electrons of europium appropriately. Including 4f electrons in the valence can reduce transferability while increasing the necessary kinetic energy cutoff.[10] Freezing the 4f electrons in the core eliminates these issues and, despite eliminating the magnetic contribution, has shown promise in modeling known lanthanide systems.[11] If 4f electrons are frozen in the core, separate pseudopotentials are needed for divalent ($4f^7$ core) and trivalent ($4f^6$ core) europium. Starting with tests of DFT parameters and a set

Received: October 18, 2023
Revised: December 18, 2023
Accepted: December 21, 2023
Published: January 12, 2024

https://doi.org/10.1021/jacs.3c11615
J. Am. Chem. Soc. 2024, 146, 2113−2121

of proposed candidates, DFT stability calculations can provide a practical number of compounds to explore experimentally.

COMPUTATIONAL METHODS

Proposing Candidates. To limit inhomogeneous broadening from isotope variations, we started with compositions containing Eu^{3+}, one or two mononuclidic cations, and a mononuclidic anion or oxygen. We excluded mononuclidic cations that are magnetic, toxic, radioactive, or in the lanthanides, leaving 12: Al^{3+}, $Au^{+/3+}$, Bi^{3+}, Cs^{+}, Na^{+}, Nb^{5+}, $P^{3+/5+}$, Rh^{3+}, Sc^{3+}, and Y^{3+}. We included O^{2-} in addition to the mononuclidic anions F^{-} and I^{-} to expand the initial search range. Oxygen should contribute little to broadening because of the high natural abundance of ^{16}O and its low mass relative to the other elements.[9] This process gave 234 ternary and quaternary combinations (e.g., Eu^{3+}–Cs^{+}–Na^{+}–F^{-}). Adding quaternary oxyfluorides and iodates brought the total to 258 combinations.

For each chemical combination, we used the pymatgen package[12] to find the 15 most likely ionic substitutions.[13] We used the default log probability threshold of 0.001, where the false positive rate for substitution in the ICSD[14] test set was near zero and the true positive rate was near 50%.[13] We then collected Materials Project database entries[15,16] for the substituted combinations (e.g., Cs_2NaNdF_6 for Nd^{3+}–Cs^{+}–Na^{+}–F^{-}). We substituted the desired ion(s) into these entries and any of their polymorphs.

From the proposed materials, we excluded options where the minimum Eu^{3+} separation for every polymorph was <3.9 Å to avoid unwanted Eu^{3+} cation interactions. We also removed candidates predicted to lie in phase diagrams that had already been thoroughly investigated experimentally. These included two fluorides not in published phase diagrams, $CsEu_3F_{10}$ and $NaEu_2F_7$;[17] Eu–Bi–O compositions in a solid-solution phase region[18] or with nonstoichiometric structures;[19] Eu–Y–O compositions expected to be solid-solutions;[20] and Eu–Al–O compounds not appearing in phase diagrams.[21,22]

Pseudopotentials. For structure relaxation, we tested PBE[23] pseudopotentials from the pslibrary set (v. 1.0.0)[10] that allow for spin–orbit coupling contributions and PBE pseudopotentials from the SSSP Efficiency set (v. 1.1.2)[24−26] that use the scalar relativistic approximation.[27−29] The pslibrary europium pseudopotentials placed the 4f electrons in the core, while the SSSP europium pseudopotential placed them in the valence. We, therefore, made the SSSP set relaxations spin-polarized. To include 4f electron bands, we also used the SSSP set for band structure calculations, following the SeeK-path conventions.[30] All pseudopotentials are listed with their recommended energy cutoffs in the Supporting Information, as are the valence configurations of each europium pseudopotential.

Structure Relaxation. Initial test runs used Quantum Espresso v.6.4.1, while final relaxation runs used v.7.0.[31−33] For final relaxations, the kinetic energy cutoff for wave functions was 952 eV (70 Ry), and the cutoff for charge density and potential was 6260 eV (460 Ry), both just above the highest recommended values among the pslibrary pseudopotentials. Structure relaxations used a Monkhorst–Pack **k**-point grid[34] initialized with a minimum of $500/n$ points (n = number of atoms in the cell) distributed in proportion to reciprocal lattice vector lengths. We required 5×10^{-5} eV/atom (3.7×10^{-6} Ry/atom) convergence for electronic relaxation, 5×10^{-4} eV/atom (3.7×10^{-5} Ry/atom) for ionic relaxation, 9.45×10^{-3} eV/Å/atom (3.7×10^{-4} Ry/a_0/atom) for forces on each atom, and 0.5 kbar pressure for cell parameters. The force convergence follows Quantum Espresso's default of 10× the ionic convergence. Similar convergence criteria have performed well for diverse chemical systems.[35] Calculations with the pslibrary set included spin–orbit coupling, and since the 4f electrons of Eu were treated as core electrons, they were not spin-polarized.

To quantify stability, we relaxed the appropriate elemental compounds (e.g., $Eu_{(s)}$). We then calculated the formation enthalpy (ΔH_f) by subtracting the total energy (E_{tot}) of each constituent elemental compound from E_{tot} of the compound of interest, with every value normalized to the number of atoms (e.g., eq 1).

$$\Delta H_{f,Cs_2NaEuF_6} = E_{tot,Cs_2NaEuF_6} - \frac{2}{10}E_{tot,Cs} - \frac{1}{10}E_{tot,Na} - \frac{1}{10}E_{tot,Eu} - \frac{6}{10}E_{tot,F} \quad (1)$$

Finally, we used the ΔH_f of the compound and its "competing" phases to calculate the energy above the hull (E_{hull}) values. Competing phases are those that are closest to a proposed compound by composition. If a competing phase has multiple known polymorphs, we considered every polymorph in our calculations. For our Eu^{2+} competing phases, we calculated the total energy with the $4f^7$ core pseudopotential and subtracted the $Eu_{(s)}$ energy also calculated with the $4f^7$ core pseudopotential to get ΔH_f, giving results consistent with published ΔH_f values (Table 1).

Table 1. Computed ΔH_f Values Best Match the Experimental Values When the Appropriate Pseudopotential Is Used for the Compound Total Energy and the Europium Metal Total Energy ($4f^6$ Core for Eu^{3+} and $4f^7$ Core for Eu^{2+})[a]

compound	ΔH_f Expt	ΔH_f $4f^6$	ΔH_f $4f^7$
EuI_2 (2+)	−1.836[36]	−1.189	−1.742
EuO (2+)	−3.057[37]	−2.492	−3.219
Eu_2O_3 (3+)	−3.446[37]	−3.629	−2.219
EuF_3 (3+)	−4.195[37]	−4.184	−3.042
$EuPO_4$ (3+)	−3.220[38]	−3.026	−2.511

[a]All ΔH_f values are in eV/atom.

EXPERIMENTAL METHODS

We collected powder X-ray diffraction (XRD) data on a Bruker D8 Advance diffractometer with capillary geometry and Mo Kα radiation. We performed Rietveld refinements to XRD data with GSAS-II.[39] Magnetic susceptibility and magnetization were measured with a Quantum Design Magnetic Property Measurement System. We placed the powder in a gel capsule mounted in a straw and used the DC measurement mode. To capture powder images and analyze chemical composition with energy dispersive X-ray spectroscopy (EDS), we spread a thin layer of powder on carbon tape and collected data with a ThermoFisher Axia ChemiSEM. We used a Nanophoton Raman 11 confocal microscope for room-temperature photoluminescence (PL) emission spectra. The instrument had a 532 nm excitation wavelength, a 50 μm slit width, and a 0.17 nm spectral resolution. We collected ten emission spectra across a sample and, seeing no variation in peak intensities, averaged the spectra to reduce noise.

RESULTS AND DISCUSSION

Pseudopotential Tests. On four Eu^{3+} chemical systems, we compared results from the relativistic pslibrary pseudopotentials ($4f^6$ frozen-core Eu) to the scalar relativistic SSSP pseudopotentials with spin polarization ($4f^6$ valence Eu). As a reference demonstrating the impact of using a europium pseudopotential with the wrong number of core 4f electrons, we also relaxed each system using the $4f^7$ frozen-core pslibrary pseudopotential meant to model Eu^{2+}. As expected, the $4f^7$ core pseudopotential does poorly for the Eu^{3+} systems. The Eu_2O_3–Al_2O_3 system is plotted in Figure 1, and the other systems are shown in the Supporting Information. For the Eu $4f^6$ core set, each experimentally reported compound is on the convex hull except $Eu_4Al_2O_9$ (E_{hull} = 1.9 meV/atom), and two unrealistic Materials Project compounds, $Eu_2Al_4O_9$ and $EuAl_{11}O_{18}$ (ion-swapped $NdAl_{11}O_{18}$), are well above it.

The $4f^6$ valence set also reproduces known phase diagrams well, but spin-polarization adds complications to calculations,

https://doi.org/10.1021/jacs.3c11615
J. Am. Chem. Soc. 2024, 146, 2113−2121

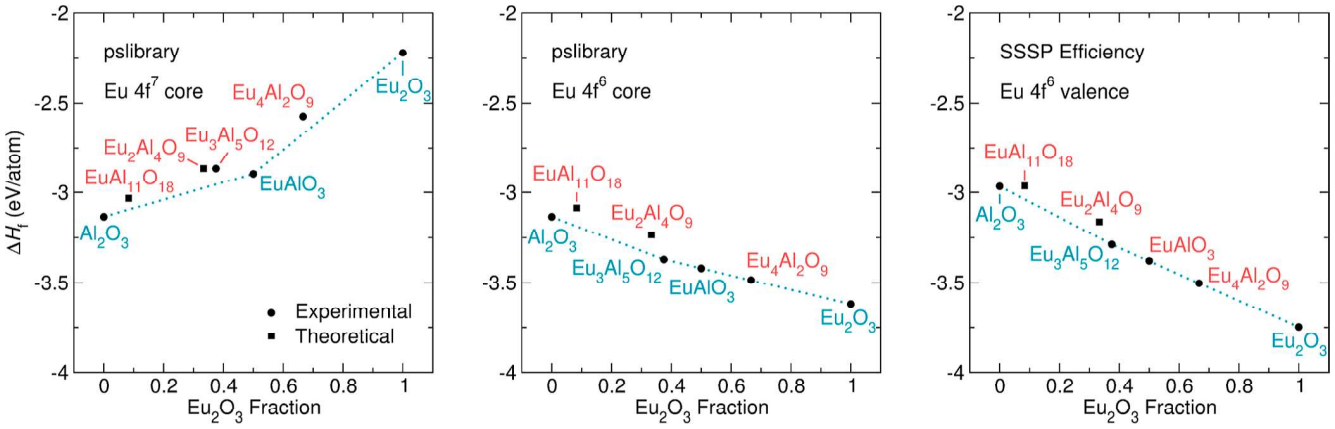

Figure 1. Three sets of pseudopotentials are tested on the Eu_2O_3–Al_2O_3 system. We assume that the binary oxides are stable. Compounds with blue labels are on the calculated hull, while those with red labels are not. Calculations using the set with $4f^6$ electrons in the Eu core place the most known compounds on the hull, though the $4f^6$ valence set also performs quite well. The known compound $Eu_4Al_2O_9$ is above the hull by 1.2 meV/atom for the $4f^6$ valence case and by 1.9 meV/atom for the $4f^6$ core case. $EuAlO_3$ is above the hull by 1.5 meV/atom for the $4f^6$ valence case.

including difficulties finding the magnetic ground state and issues accurately predicting insulating behavior without a Hubbard U. This, for example, prevented the energy convergence of the known compound $Eu_3(PO_4)O_3$ when testing several magnetic ground states or when allowing for unrestricted relaxation. Therefore, we used the pslibrary set with 4f electrons in the europium core for our structure relaxations because it reproduces known phase diagrams well and avoids spin-polarized calculations. For band structure calculations, we used the $4f^6$ valence set.

Stable Compounds. We obtained prediction results for 33 proposed structures with 19 unreported stoichiometric compositions, along with results for 48 polymorphs of 35 competing phases. Likely because the initial ion substitution did not alter the original lattice parameters, several compounds struggled to converge without a change in the initial parameters. To get a rough relaxation, we used the graph neural network interatomic potential M3GNet[40] to relax them to a better starting point. The affected compounds and their provenance were $Eu_2P_4O_{13}$ (mp-771342), $Eu_2P_4O_{13}$ (mp-772787), $EuNb_3O_9$ (mp-1173575), and $EuNb_3O_9$ (mp-1210059). Calculation results for every proposed and competing structure, as well as a CIF for each relaxed proposed structure, are provided in the Supporting Information. Several proposed structures were predicted to be stable. The noniodide ones are listed in Table 2 with their energy relative to the convex hull if it were constructed without them (E_{rel}), and their crystal structures are shown in the Supporting Information.

Several observations about the proposed compounds should be made before discussing synthesis attempts. First, two iodide compounds were predicted to be stable, $Cs_3Eu_2I_9$ and Na_3EuI_6, but we did not attempt to synthesize them because there are no known Eu^{3+} iodides. EuI_3 has not been realized experimentally[41,42] as its hydrated phases decompose directly into EuI_2,[43,44] and it has an estimated formation enthalpy ~0.6 eV/atom higher than that of EuI_2.[36,45,46] Also, while Na_3MI_6 has been synthesized for M = Sm, Gd, Tb, and Dy, Na_3EuI_6 is conspicuously absent.[47] Second, the quaternary fluoride Cs_2NaEuF_6 has a nonpolar predicted europium site symmetry that should preclude observation of the $^5D_0 \rightarrow {}^7F_0$ transition; however, the composition's actual structure, if synthesized, may of course be different. Finally, before completing the calculations, we were unaware of the prior report of $Eu_2P_4O_{13}$,[48] which is not in ICSD or the Materials Project. We calculated energies for four proposed polymorphs of the compound, and the most stable is the same as that realized experimentally. Only polycrystalline $Eu_2P_4O_{13}$ was previously synthesized by decomposition of $Eu(PO_3)_3$, so we did not pursue crystal growth here because of the complicated phase space. The relaxed volume of $Eu_2P_4O_{13}$ (1109.96 Å^3) was 3.6% larger than the experimental volume (1071.66 Å^3), a common feature of PBE calculations.[49−52] The band structure of $Eu_2P_4O_{13}$ is plotted in the Supporting Information.

Table 2. Noniodide Compounds Predicted to be Stable (E_{hull} = 0) Are Listed along with Their Formation Energy Relative to the Convex Hull if It Were Constructed without Them (E_{rel})[a]

compound	E_{rel} (eV/atom)	Eu^{3+} site symmetry	Eu^{3+} separation (Å)
$Cs_3Eu(PO_4)_2$	−0.057	C_1	5.42
$CsEuP_2O_7$	−0.035	C_1	5.59
Cs_2NaEuF_6	−0.033	O_h (x)	6.52
$Eu_2P_4O_{13}$	−0.023	C_1	4.02
$Na_7Eu_2(P_2O_7)_2(P_3O_{10})$	−0.005	C_1	5.48
Cs_5EuO_4	−0.003	C_1	6.15

[a]Also listed are the predicted symmetry and separation of Eu^{3+} cations. Site symmetries followed by "(x)" are, in theory, not compatible with observing the $^5D_0 \rightarrow {}^7F_0$ transition.

Synthesis of Predicted Compounds. We successfully synthesized polycrystalline Cs_2NaEuF_6. We first combined stoichiometric amounts of CsF (99.9%, Sigma-Aldrich), EuF_3 (99.9%, Fisher), and NaF (99.99%, Alfa Aesar) under argon. We then placed them in a carbon-coated quartz tube before sealing the hygroscopic powder under vacuum. We heated the powder at 10 °C/min to 600 °C, held it at that temperature for 4 h, and cooled it back to room temperature at 10 °C/min. The structure matched the cubic double perovskite structure type used in the DFT calculations (Figure 2). The XRD pattern is shown in Figure 3, and the refined atomic positions are listed in Table 3. The refined lattice parameter is a = 9.1430(2) Å, which is smaller than the DFT predicted value of 9.2306 Å, and the experimental Eu^{3+} separation is 6.47 Å. The XRD pattern did not change over two months, showing the

https://doi.org/10.1021/jacs.3c11615
J. Am. Chem. Soc. 2024, 146, 2113−2121

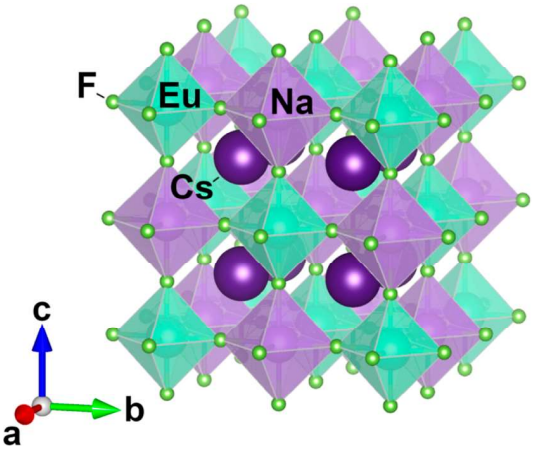

Figure 2. The double perovskite crystal structure of Cs_2NaEuF_6 is shown (a = 9.1430 Å). Cesium polyhedra are not shown to avoid crowding in the image. NaF_6 octahedra are on the cell edges and in the cell center, and EuF_6 octahedra are on the cell faces and corners.

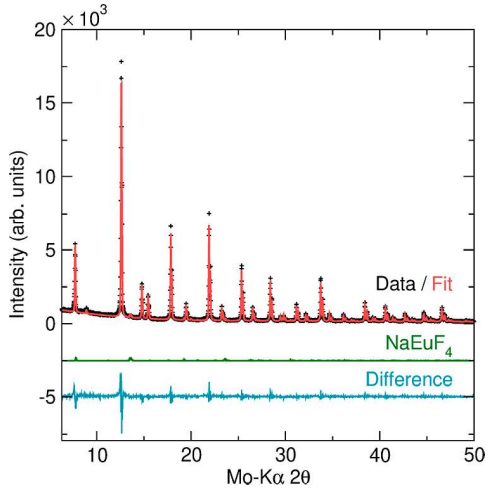

Figure 3. A powder XRD refinement of Cs_2NaEuF_6 is shown and includes a small $NaEuF_4$ impurity (1.7 wt %). Including Cs/Na site mixing did not improve the fit.

Table 3. Refined Atomic Positions for Cs_2NaEuF_6 Are Listed (Space Group $Fm\bar{3}m$, a = 9.1430(2) Å)

atom	site	x	y	z
Cs	8c	0.25	0.25	0.25
Na	4b	0	0	0.5
Eu	4a	0	0	0
F	24e	0	0	0.248(1)

fluoride's air stability (Supporting Information). A small $NaEuF_4$ impurity that we could not eliminate with excess CsF was present in each sample.

Next, we attempted to grow Cs_2NaEuF_6 single crystals by melting the starting powders in a carbon-coated tube and slowly cooling through the melting point. As the melting point of the mixture is unknown, we attempted to heat the mixture to 700 °C. At this temperature, though, the compound attacks the glass despite the carbon coating, eliminating that route to single crystals. Additionally, EuF_3 is insoluble in water, precluding simple solution precipitation. The most likely routes to high-quality single crystals are a hydrofluoric acid solution method or a high-temperature sealed metal tube method.

To characterize the magnetic properties of Cs_2NaEuF_6, we collected field-cooled and zero-field-cooled magnetic susceptibility data from 2 to 395 K at 10 kOe on a 38.1 mg powder sample (Figure 4). The compound is a Van Vleck paramagnet, having a temperature-independent susceptibility at lower temperatures. The field-cooled and zero-field-cooled data did not deviate from each other. As observed in other Eu^{3+} compounds,[53] the data had a Curie tail near the base temperature due to Eu^{2+} impurities. Fitting to a Van Vleck model[53,54] above 55 K gives an energy separation between the $^7F_0$ and $^7F_1$ levels (λ) of 43.6 meV (λ/k_B = 506 K), which agrees with the PL emission spectrum discussed below. The corresponding magnetization curves are linear with no hysteresis, as expected for a paramagnet (Figure 4).

The band structure of Cs_2NaEuF_6 is shown in Figure 5. With increasing Hubbard U,[55,56] several highly localized 4f bands are shifted higher in energy, increasing the band gap. With a U of 10 eV, similar to values successfully used to model lanthanide sesquioxides,[57,58] the band gap is 5.0 eV. Decreasing U leads to a linear decrease in the gap (E_{gap} = 1.4, 2.3, 3.2, or 4.0 eV for U = 2, 4, 6, or 8 eV, respectively). The Supporting Information contains the band structure for the $4f^6$ core pseudopotential case for comparison. The Cs_2NaEuF_6 polycrystalline product was white-gray, which supports a larger gap prediction.

When the sealed tube contained starting powders in a boron nitride crucible and excess CsF in a separate crucible, the excess CsF had a darker hue after synthesis. EDS revealed oxygen contamination in the perovskite product (Supporting Information). The gray hue, therefore, likely comes from the oxygen contamination or Eu^{2+} impurities, but no unidentified peaks were present in our XRD patterns.

On a Cs_2NaEuF_6 powder sample, we collected room-temperature PL emission data (Figure 6). Because of the O_h site symmetry of Eu^{3+}, we would expect to observe only the $^5D_0 \rightarrow {}^7F_1$ transition with one peak.[59] Instead, we see each of the $^5D_0 \rightarrow {}^7F_J$ (J = 0–4) transitions, with the J = 1–4 transitions having multiple peaks and one of the three J = 1 peaks being the most intense. Many symmetry-lowering factors can lead to observing the additional transitions, including site disorder in the $NaEuF_4$ impurity,[60] oxygen or Eu^{2+} defects in the structure, or other defects. In the spectrum, the wavenumber shift between the observed $^5D_0 \rightarrow {}^7F_1$ and $^5D_0 \rightarrow {}^7F_0$ transitions is 365 cm^{-1} (45.3 meV), which is close to the 43.6 meV energy separation between the $^7F_0$ and $^7F_1$ levels calculated from magnetometry data.

We attempted several solid-state crystal growth methods for $Cs_3Eu(PO_4)_2$. The first followed a procedure for $Cs_3Ln(PO_4)_2$ (Ln = Y, Gd) that uses a Cs_2CO_3–H_3BO_3 flux.[61] After rinsing the flux off with water, we recovered only anamorphous product. The second procedure adapted a $Rb_3Ln(PO_4)_2$ (Ln = Y, Dy–Lu) growth procedure[62] by using a eutectic Cs_2CO_3–CsF flux with $(NH_4)_2HPO_4$ and Eu_2O_3 in the stoichiometric ratio. After the flux was rinsed off with water, only Eu_2O_3 remained. Additional details are in the Supporting Information.

To try to grow $CsEuP_2O_7$ crystals, we replaced the lanthanide precursor with europium compounds for several solution[63,64] and solid-state[65,66] synthesis procedures for isostructural lanthanide compounds. None of the procedures returned a phase containing Cs, Eu, P, and O. Both solid-state procedure products contained $EuPO_4$, with one including a

https://doi.org/10.1021/jacs.3c11615
J. Am. Chem. Soc. 2024, 146, 2113–2121

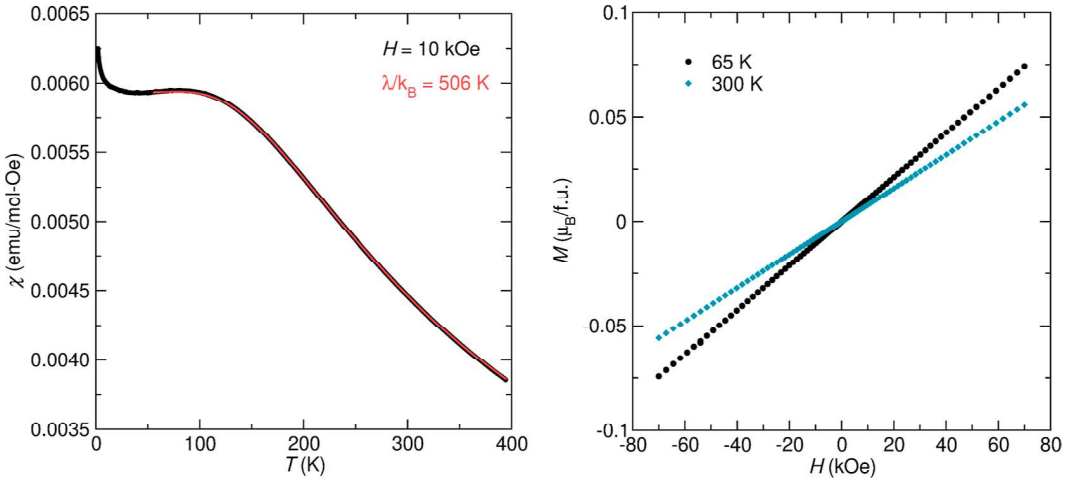

Figure 4. (Left) The field-cooled magnetic susceptibility of Cs_2NaEuF_6 is shown along with a Van Vleck susceptibility model fit. The data and fit show good agreement until near 55 K, where Eu^{2+} impurities create a Curie tail at lower temperatures. Data points are indistinguishable because of their tight spacing. (Right) The isothermal magnetization curves for paramagnetic Cs_2NaEuF_6 at 65 and 300 K are linear and show no hysteresis (f.u. = formula unit).

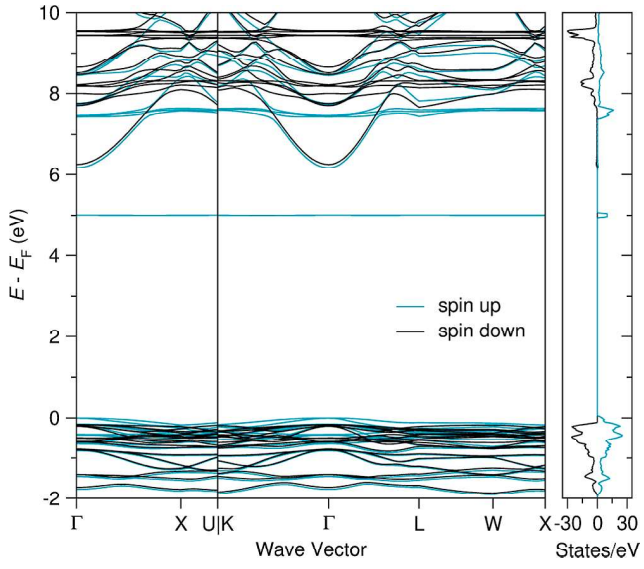

Figure 5. The spin-polarized band structure of Cs_2NaEuF_6, calculated with the $4f^6$ valence pseudopotential set and U = 10 eV, is plotted with the density of states. The band gap is 5.0 eV. The Fermi energy is defined as the highest occupied state, and the spin-down density of states is negative.

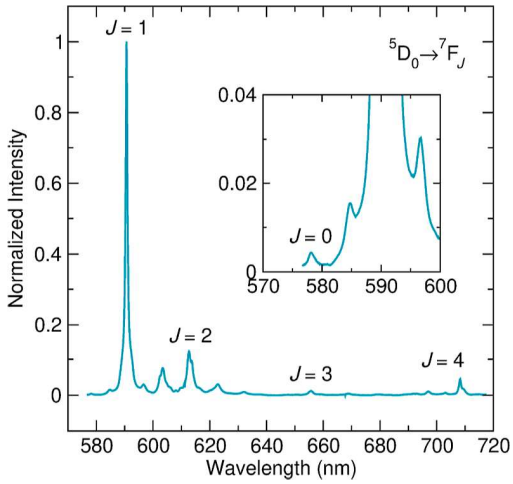

Figure 6. The room-temperature PL emission spectrum of Cs_2NaEuF_6 shows each of the $^5D_0 \rightarrow {}^7F_J$ (J = 0–4) transitions. The inset shows the weak J = 0 transition next to the much higher-intensity J = 1 transition and its shoulder peaks.

small $EuPO_4$ crystal. The crystal's PL emission spectrum, with a sharp $^5D_0 \rightarrow {}^7F_0$ transition matching a previous study,[67] is in the Supporting Information along with additional synthesis attempt details.

For $Na_7Eu_2(P_2O_7)_2(P_3O_{10})$, we followed the procedure used for its only reported isostructural compound, $Na_7Y_2(P_2O_7)_2(P_3O_{10})$.[68] The resulting product also contained $EuPO_4$, along with unidentifiable phase(s). The XRD pattern is in the Supporting Information along with synthesis attempt details. $EuPO_4$ again appears to be more energetically favorable than the predicted alkali-europium-phosphate compound.

Finally, we attempted to synthesize Cs_5EuO_4 by heating a stoichiometric mixture of Cs_2CO_3 and Eu_2O_3 in an alumina crucible. After 48 h at 1000 °C, only Eu_2O_3 remained. We believe that Cs_2CO_3 decomposed to Cs_2O, which then evaporated since it was well above its melting point.

Other Materials Project Database Candidates. In addition to screening proposed candidates with DFT, we searched for existing entries in the Materials Project. First, using the database's API,[16] we queried every binary, ternary, and quaternary entry that contained the ions we used to propose structures. Then, we filtered out entries with a Eu^{3+} minimum separation less than 3.95 Å and entries with nonpolar Eu^{3+} site symmetries. After filtering, seven compounds remained, each experimentally realized. They are given in Table 4. Their database IDs are listed in the Supporting Information, as are compounds with a smaller Eu^{3+} separation. Six of the seven are phosphates, which stem from our chemistry restrictions. Phosphorus, unlike the other cations, consistently forms polyatomic ions with oxygen. These polyatomic ions exist in various geometries (see extensive overviews[69−71]) that allow for large Eu^{3+} cation separation and

https://doi.org/10.1021/jacs.3c11615
J. Am. Chem. Soc. 2024, 146, 2113−2121

Table 4. Listed Are Materials Project Entries (v2022.10.28) with Eu^{3+} Separations ≥ 3.95 Å, the Desired Elements, and Eu^{3+} Site Symmetries Compatible with Observing the $^5D_0 \rightarrow {}^7F_0$ Transition[a]

compound	MP E_{hull} (eV/atom)	Eu^{3+} site symmetry	MP Eu^{3+} separation (Å)	$^5D_0$ lifetime[b]
$CsEu(PO_3)_4$	0.021	C_1	5.85	~3.2 μs[c] (77 K)[72]
$NaEu(PO_3)_4$	0.025	C_1	5.78	~4.8 μs[c] (77 K)[72]
EuP_5O_{14}	0.019	C_1	5.16	4.4 ms (100 K)[73] 4.8 ms[74,75]
$NaEuP_2O_7$	0	C_1	4.34	
$Eu(IO_3)_3$	0	C_1	4.31	1.6 ms (4.2 K)[76]
$Eu(PO_3)_3$[d]	0	C_2	4.20	3.39 ms[77]
$EuPO_4$	0	C_1	4.05	~0.81 ms[67]

[a]For several lifetimes, the collection temperature is unclear. [b]Values preceded by "~" are estimated from graphs. [c]See the main text note about reliability. [d]See the main text about the high-temperature polymorph with a larger Eu^{3+} separation.

provide space for the mononuclidic alkali metal cations Na^+ and Cs^+.

Encouragingly, six of the seven compounds have reported crystal growth procedures, and all seven compounds have reported $^5D_0 \rightarrow {}^7F_0$ Eu^{3+} transitions: $CsEu(PO_3)_4$,[72,78] $NaEu(PO_3)_4$,[72,79] EuP_5O_{14},[73,74,80] $NaEuP_2O_7$,[79] $Eu(IO_3)_3$,[76,81,82] $Eu(PO_3)_3$,[77] and $EuPO_4$ (cf. Supporting Information).[67,83] For the Materials Project $Eu(PO_3)_3$ entry (space group $C222_1$), we could only find reports of polycrystalline samples.[48,77,84,85] However, single crystals are reported for a high-temperature $Eu(PO_3)_3$ polymorph (space group $C2/c$) with a $^5D_0 \rightarrow {}^7F_0$ active Eu^{3+} site symmetry (C_1) and a minimum Eu^{3+} separation of 5.30 Å.[48] Two of the phosphate candidates were studied together, showing a more intense $^5D_0 \rightarrow {}^7F_0$ peak for $NaEuP_2O_7$ than that for $NaEu(PO_3)_4$.[79] To our knowledge, only EuP_5O_{14} has a reported $^5D_0 \rightarrow {}^7F_0$ inhomogeneous linewidth, 3.5 GHz, and optical coherence time, 10 μs.[86] Though much larger than needed to resolve hyperfine energy levels (~70−140 MHz), this linewidth is similar to or lower than that of europium-doped systems[87−90] while providing a drastically higher europium concentration. The line profile was also asymmetric, and the linewidth varied across the crystal, indicating strain and crystal homogeneity contributed to broadening.[86]

Except for $NaEuP_2O_7$, each compound also has a reported optical lifetime for the $^5D_0$ energy level. Measurement temperature ambiguity complicates direct comparisons, especially for phonon-mediated effects. Still, the $^5D_0$ decay time of EuP_5O_{14} is the largest at 4.8 ms.[74,75] The 3.39 ms lifetime for $Eu(PO_3)_3$, interestingly, increases for doped $(Y_{1-x}, Eu_x)(PO_3)_3$, indicating that the 4.2 Å Eu^{3+} separation in the undoped sample leads to a high energy transfer probability.[77] Focusing on compounds with a Eu^{3+} separation ≥4.2 Å may therefore be prudent; however, for stoichiometric quantum memory, the more critical factor is whether the optical coherence time approaches the optical lifetime limit. Also, of note, the microsecond-scale lifetimes of $CsEu(PO_3)_4$ and $NaEu(PO_3)_4$ may be inaccurate as the report also gives a ~4.4 μs lifetime for $KEu(PO_3)_4$, while others report 4.02 ms.[91]

Because ^{31}P has the lowest nuclear spin $\left(I = \frac{1}{2}\right)$ of the cations included in the search, phosphates are well-suited for these applications. Additionally, EuP_5O_{14}, $Eu(PO_3)_3$, and $EuPO_4$ do not involve large nuclear spins from ^{133}Cs $\left(I = \frac{7}{2}\right)$ or ^{23}Na $\left(I = \frac{3}{2}\right)$. The reduced nuclear spin baths may help explain the longer reported lifetimes of the Eu−P−O compounds, but a single crystal study of each candidate under consistent experimental conditions is necessary for a more thorough comparison.

In summary, each compound is a promising candidate. EuP_5O_{14} has benchmark values for its inhomogeneous linewidth and optical coherence time. $Eu(PO_3)_3$ and $Eu(IO_3)_3$ have millisecond-scale optical lifetimes. $EuPO_4$ and $NaEuP_2O_7$ have noticeable $^5D_0 \rightarrow {}^7F_0$ transitions at room temperature. Also, the $MEu(PO_3)_4$ compounds have large Eu^{3+} separation and may have longer than reported excited state lifetimes. $Eu(IO_3)_3$ has the additional advantage of avoiding phosphate chemistry, which can be plagued by synthesis complications related to producing crystals with the desired phosphate polyatomic ion.

CONCLUSIONS

We have explored several new stoichiometric candidates for optically addressable quantum memory systems that would not require isotopic enrichment and that have a large europium separation. We initially proposed 33 theoretical structures with 19 unrealized compositions. We then showed that using fully relativistic $4f^6$ and $4f^7$ frozen-core pseudopotentials for Eu^{3+} and Eu^{2+}, respectively, provided accurate predictions of europium system ΔH_f values. Using DFT calculations, we predicted that six of the unrealized compositions have a stable polymorph, including $Eu_2P_4O_{13}$, which, unknown to us beforehand, has been synthesized.

We then successfully synthesized the DFT-predicted compound Cs_2NaEuF_6, an air-stable and insulating double perovskite halide with a large Eu^{3+} separation that leads to paramagnetic behavior. Magnetic susceptibility, optical spectra, and EDS indicate that the compound contains several defects. Though our attempts to synthesize the other predicted compounds were unsuccessful, we believe more extensive tests are merited for $Cs_3Eu(PO_4)_2$ and $CsEuP_2O_7$ because of the compounds' favorable Eu^{3+} separations and site symmetries as well as the wide range of tunable synthesis parameters involved.

In addition to our predicted compounds, we evaluated the Materials Project entries to find unexplored chemical spaces containing more stoichiometric candidates. Six known phosphate compounds and one iodate have large Eu^{3+} separations, appropriate Eu^{3+} site symmetries, and advantageous reported optical properties. The inhomogeneous linewidths of each, except EuP_5O_{14}, are unstudied.

To implement dense, optically addressable quantum memory with stoichiometric compounds, finding environmentally stable materials with controlled or minimal defect chemistry remains critical. The diversity of Eu^{3+} stoichiometric systems necessitates data-driven approaches to finding promising candidates. This work demonstrates a pathway to accurate stability predictions and provides a new set of compounds to prioritize in future studies.

https://doi.org/10.1021/jacs.3c11615
J. Am. Chem. Soc. 2024, 146, 2113−2121

■ ASSOCIATED CONTENT

Supporting Information

The Supporting Information is available free of charge at https://pubs.acs.org/doi/10.1021/jacs.3c11615.

Initial valence configurations of each Eu pseudopotential; relativistic pseudopotentials from the pslibrary v. 1.0.0 set; scalar relativistic pseudopotentials from the SSSP Efficiency v. 1.1.2 set; proposed compound DFT results and structural information; competing compound DFT results and structural information; competing compounds and original structures associated with each proposed phase; Materials Project entries with small Eu^{3+} separation; database IDs for Materials Project entries with large Eu^{3+} separation; additional pseudopotential test systems; comparison of experimental and theoretical ΔH_f and cell volume values for competing phases; crystal structures of the six DFT-predicted stable compounds; comparison of Cs_2NaEuF_6 band structures calculated with and without 4f electrons in the valence; comparison of $Eu_2P_4O_{13}$ band structures calculated with and without 4f electrons in the valence; XRD pattern stability of Cs_2NaEuF_6 over two months; SEM images of Cs_2NaEuF_6 powder used for EDS data collection; EDS spectra of a Cs_2NaEuF_6 powder sample; XRD refinements of products from unsuccessful synthesis procedures for DFT-predicted compounds; and a PL emission spectrum of a $EuPO_4$ crystal (PDF)

CIFs containing the DFT-relaxed structures for each proposed compound (ZIP)

Accession Codes

CCDC 2302012 contains the supplementary crystallographic data for this paper. These data can be obtained free of charge via www.ccdc.cam.ac.uk/data_request/cif, by emailing data_request@ccdc.cam.ac.uk, or by contacting the Cambridge Crystallographic Data Centre, 12 Union Road, Cambridge CB2 1EZ, UK; fax: +44 1223 336033.

■ AUTHOR INFORMATION

Corresponding Author

Daniel P. Shoemaker − *Department of Materials Science and Engineering, University of Illinois Urbana—Champaign, Urbana, Illinois 61801, United States; Materials Research Laboratory, University of Illinois Urbana—Champaign, Urbana, Illinois 61801, United States;* orcid.org/0000-0003-3650-7551; Email: dpshoema@illinois.edu

Author

Zachary W. Riedel − *Department of Materials Science and Engineering, University of Illinois Urbana—Champaign, Urbana, Illinois 61801, United States; Materials Research Laboratory, University of Illinois Urbana—Champaign, Urbana, Illinois 61801, United States;* orcid.org/0000-0001-5848-5520

Complete contact information is available at: https://pubs.acs.org/10.1021/jacs.3c11615

Notes

The authors declare no competing financial interest.

■ ACKNOWLEDGMENTS

We are grateful for helpful conversations with Elif Ertekin and André Schleife about our DFT procedures and with Elizabeth Goldschmidt about quantum memory applications. DFT calculations were performed on the High Throughput Computing Pilot Program at the University of Illinois Urbana—Champaign. Optical characterization was performed at the Materials Research Laboratory Central Research Facilities at the University of Illinois. The authors acknowledge the use of facilities and instrumentation supported by NSF through the University of Illinois Materials Research Science and Engineering Center DMR-1720633. This work was supported by the U.S. Department of Energy, Office of Science, National Quantum Information Science Research Center Q-NEXT. Z.W.R. was supported by the National Science Foundation under grant no. 1922758 (DIGI-MAT).

■ REFERENCES

(1) Könz, F.; Sun, Y.; Thiel, C.; Cone, R.; Equall, R.; Hutcheson, R.; Macfarlane, R. Temperature and concentration dependence of optical dephasing, spectral-hole lifetime, and anisotropic absorption in Eu^{3+}:Y_2SiO_5. *Phys. Rev. B: Condens. Matter Mater. Phys.* **2003**, *68*, 085109.

(2) Longdell, J. J.; Fraval, E.; Sellars, M. J.; Manson, N. B. Stopped light with storage times greater than one second using electromagnetically induced transparency in a solid. *Phys. Rev. Lett.* **2005**, *95*, 063601.

(3) Böttger, T.; Thiel, C.; Cone, R.; Sun, Y. Effects of magnetic field orientation on optical decoherence in Er^{3+}:Y_2SiO_5. *Phys. Rev. B: Condens. Matter Mater. Phys.* **2009**, *79*, 115104.

(4) Zhong, M.; Hedges, M. P.; Ahlefeldt, R. L.; Bartholomew, J. G.; Beavan, S. E.; Wittig, S. M.; Longdell, J. J.; Sellars, M. J. Optically addressable nuclear spins in a solid with a six-hour coherence time. *Nature* **2015**, *517*, 177−180.

(5) Ahlefeldt, R. L.; Pearce, M. J.; Hush, M. R.; Sellars, M. J. Quantum processing with ensembles of rare-earth ions in a stoichiometric crystal. *Phys. Rev. A* **2020**, *101*, 012309.

(6) Ahlefeldt, R. L.; Smith, A.; Sellars, M. J. Ligand isotope structure of the optical $^7F_0 \rightarrow {}^5D_0$ transition in $EuCl_3{\cdot}6H_2O$. *Phys. Rev. B: Condens. Matter Mater. Phys.* **2009**, *80*, 205106.

(7) Ahlefeldt, R. L.; Manson, N. B.; Sellars, M. J. Optical lifetime and linewidth studies of the $^7F_0 \rightarrow {}^5D_0$ transition in $EuCl_3{\cdot}6H_2O$: A potential material for quantum memory applications. *J. Lumin.* **2013**, *133*, 152−156.

(8) Ahlefeldt, R. L.; McAuslan, D. L.; Longdell, J. J.; Manson, N. B.; Sellars, M. J. Precision Measurement of Electronic Ion-Ion Interactions between Neighboring Eu^{3+} Optical Centers. *Phys. Rev. Lett.* **2013**, *111*, 240501.

(9) Ahlefeldt, R.; Hush, M. R.; Sellars, M. Ultranarrow optical inhomogeneous linewidth in a stoichiometric rare-earth crystal. *Phys. Rev. Lett.* **2016**, *117*, 250504.

(10) Dal Corso, A. Pseudopotentials periodic table: From H to Pu. *Comput. Mater. Sci.* **2014**, *95*, 337−350.

(11) Gao, M. C.; Rollett, A. D.; Widom, M. Lattice stability of aluminum-rare earth binary systems: A first-principles approach. *Phys. Rev. B: Condens. Matter Mater. Phys.* **2007**, *75*, 174120.

(12) Ong, S. P.; Richards, W. D.; Jain, A.; Hautier, G.; Kocher, M.; Cholia, S.; Gunter, D.; Chevrier, V. L.; Persson, K. A.; Ceder, G. Python Materials Genomics (pymatgen): A robust, open-source python library for materials analysis. *Comput. Mater. Sci.* **2013**, *68*, 314−319.

(13) Hautier, G.; Fischer, C.; Ehrlacher, V.; Jain, A.; Ceder, G. Data mined ionic substitutions for the discovery of new compounds. *Inorg. Chem.* **2011**, *50*, 656−663.

(14) Belsky, A.; Hellenbrandt, M.; Karen, V. L.; Luksch, P. New developments in the Inorganic Crystal Structure Database (ICSD): accessibility in support of materials research and design. *Acta Crystallogr., Sect. B: Struct. Sci.* **2002**, *58*, 364−369.

(15) Jain, A.; Ong, S. P.; Hautier, G.; Chen, W.; Richards, W. D.; Dacek, S.; Cholia, S.; Gunter, D.; Skinner, D.; Ceder, G.; et al.

Commentary: The Materials Project: A materials genome approach to accelerating materials innovation. *APL Mater.* **2013**, *1*, 011002.
(16) Ong, S. P.; Cholia, S.; Jain, A.; Brafman, M.; Gunter, D.; Ceder, G.; Persson, K. A. The Materials Application Programming Interface (API): A simple, flexible and efficient API for materials data based on REpresentational State Transfer (REST) principles. *Comput. Mater. Sci.* **2015**, *97*, 209−215.
(17) Fedorov, P. P. Systems of alkali and rare-earth metal fluorides. *Zh. Neorg. Khim.* **1999**, *44*, 1792−1818.
(18) Turkoglu, O.; Soylak, M.; Belenli, I. Synthesis and characterization of β type solid solution in the binary system of Bi_2O_3-Eu_2O_3. *Bull. Mater. Sci.* **2002**, *25*, 583−588.
(19) Saha, S.; Chanda, S.; Dutta, A.; Kumar, U.; Ranjan, R.; Sinha, T. P. Dielectric relaxation and anti-ferromagnetic coupling of $BiEuO_3$ and $BiGdO_3$. *J. Magn. Magn. Mater.* **2014**, *360*, 80−86.
(20) Andrievskaya, E. R.; Zaitseva, Z. A.; Shevchenko, A. V.; Lopato, L. M. Phase diagram of the Eu_2O_3-Y_2O_3 system. *Inorg. Mater.* **1997**, *33*, 390−393.
(21) Mizuno, M.; Yamada, T.; Noguchi, T. Phase diagrams of the systems Al_2O_3-Eu_2O_3 and Al_2O_3-Gd_2O_3 at high temperatures. *Yogyo Kyokaishi* **1977**, *85*, 374−379.
(22) Wu, P.; Pelton, A. D. Coupled thermodynamic-phase diagram assessment of the rare earth oxide-aluminium oxide binary systems. *J. Alloys Compd.* **1992**, *179*, 259−287.
(23) Perdew, J. P.; Burke, K.; Ernzerhof, M. Generalized gradient approximation made simple. *Phys. Rev. Lett.* **1996**, *77*, 3865−3868.
(24) Lejaeghere, K.; Bihlmayer, G.; Björkman, T.; Blaha, P.; Blügel, S.; Blum, V.; Caliste, D.; Castelli, I. E.; Clark, S. J.; Dal Corso, A.; et al. Reproducibility in density functional theory calculations of solids. *Science* **2016**, *351*, aad3000.
(25) Prandini, G.; Marrazzo, A.; Castelli, I. E.; Mounet, N.; Marzari, N. Precision and efficiency in solid-state pseudopotential calculations. *npj Comput. Mater.* **2018**, *4*, 72.
(26) Prandini, G.; Marrazzo, A.; Castelli, I. E.; Mounet, N.; Passaro, E.; Marzari, N. *A Standard Solid State Pseudopotentials (SSSP) Library Optimized for Precision and Efficiency*, 2021..
(27) Koelling, D. D.; Harmon, B. N. A technique for relativistic spin-polarised calculations. *J. Phys. C: Solid State Phys.* **1977**, *10*, 3107−3114.
(28) Gollisch, H.; Fritsche, L. Relativistic one-particle equation for electron states of heavy metals. *Phys. Status Solidi B* **1978**, *86*, 145−150.
(29) Takeda, T. The scalar relativistic approximation. *Z. Phys. B: Condens. Matter* **1978**, *32*, 43−48.
(30) Hinuma, Y.; Pizzi, G.; Kumagai, Y.; Oba, F.; Tanaka, I. Band structure diagram paths based on crystallography. *Comput. Mater. Sci.* **2017**, *128*, 140−184.
(31) Giannozzi, P.; Baroni, S.; Bonini, N.; Calandra, M.; Car, R.; Cavazzoni, C.; Ceresoli, D.; Chiarotti, G. L.; Cococcioni, M.; Dabo, I.; et al. QUANTUM ESPRESSO: a modular and open-source software project for quantum simulations of materials. *J. Phys.: Condens. Matter* **2009**, *21*, 395502.
(32) Giannozzi, P.; Andreussi, O.; Brumme, T.; Bunau, O.; Buongiorno Nardelli, M.; Calandra, M.; Car, R.; Cavazzoni, C.; Ceresoli, D.; Cococcioni, M.; et al. Advanced capabilities for materials modelling with Quantum ESPRESSO. *J. Phys.: Condens. Matter* **2017**, *29*, 465901.
(33) Giannozzi, P.; Baseggio, O.; Bonfà, P.; Brunato, D.; Car, R.; Carnimeo, I.; Cavazzoni, C.; De Gironcoli, S.; Delugas, P.; Ferrari Ruffino, F.; et al. Quantum ESPRESSO toward the exascale. *J. Chem. Phys.* **2020**, *152*, 154105.
(34) Monkhorst, H. J.; Pack, J. D. Special points for Brillouin-zone integrations. *Phys. Rev. B: Solid State* **1976**, *13*, 5188−5192.
(35) Jain, A.; Hautier, G.; Moore, C. J.; Ping Ong, S.; Fischer, C. C.; Mueller, T.; Persson, K. A.; Ceder, G. A high-throughput infrastructure for density functional theory calculations. *Comput. Mater. Sci.* **2011**, *50*, 2295−2310.
(36) Wicks, C. E.; Block, F. E. *Thermodynamic Properties of 65 Elements: Their Oxides, Halides, Carbides and Nitrides*; US Government Printing Office, 1963; Vol. *605*.
(37) *Materials Thermochemistry*, 6th ed.; Kubaschewski, O., Ed.; Pergamon Press: New York, 1993.
(38) Popa, K.; Konings, R. J. M. High-temperature heat capacities of $EuPO_4$ and $SmPO_4$ synthetic monazites. *Thermochim. Acta* **2006**, *445*, 49−52.
(39) Toby, B. H.; Von Dreele, R. B. GSAS-II: the genesis of a modern open-source all purpose crystallography software package. *J. Appl. Crystallogr.* **2013**, *46*, 544−549.
(40) Chen, C.; Ong, S. P. A universal graph deep learning interatomic potential for the periodic table. *Nat. Comput. Sci.* **2022**, *2*, 718−728.
(41) Asprey, L. B.; Keenan, T. K.; Kruse, F. H. Preparation and crystal data for lanthanide and actinide triiodides. *Inorg. Chem.* **1964**, *3*, 1137−1141.
(42) Wetzel, K. In *Handbook of Preparative Inorganic Chemistry*; Brauer, G., Ed.; Academic Press: New York, 1963; p 1150.
(43) Jenden, C. M.; Lyle, S. J. A Mössbauer spectroscopic study of the Iodides of europium. *J. Chem. Soc., Dalton Trans.* **1982**, 2409−2414.
(44) Diao, C.; Yu, J.; Li, H.; Peng, P.; Wu, H.; He, H.; Yan, S.; Hu, Y. Ammonium-iodide route to anhydrous EuI_2: mechanism and preparation. *J. Rare Earths* **2015**, *33*, 1189−1195.
(45) Kirklin, S.; Saal, J. E.; Meredig, B.; Thompson, A.; Doak, J. W.; Aykol, M.; Rühl, S.; Wolverton, C. The Open Quantum Materials Database (OQMD): assessing the accuracy of DFT formation energies. *npj Comput. Mater.* **2015**, *1*, 15010−15015.
(46) Meyer, G. Small cause−Great effect: What the $4f^{n+1}5d^0 \rightarrow 4f^n5d^1$ configuration crossover does to the chemistry of divalent rare-earth halides and coordination compounds. *J. Solid State Chem.* **2019**, *270*, 324−334.
(47) Bohnsack, A.; Meyer, G. Ternäre Halogenide vom Typ A_3MX_6. V. Synthese, Kristallstrukturen und Natrium-Ionenleitfähigkeit der ternären Iodide Na_3MI_6 (M = Sm, Gd−Dy) sowie der Mischkristalle $Na_3GdBr_{6-x}I_x$. *Z. Anorg. Allg. Chem.* **1997**, *623*, 837−843.
(48) Grunwald, W.; Wittich, K.; Glaum, R. Anhydrous Europium Phosphates: A Comprehensive Report on Syntheses, Crystal Structures, and Phase Relations. *Z. Anorg. Allg. Chem.* **2018**, *644*, 1403−1414.
(49) Schimka, L.; Harl, J.; Kresse, G. Improved hybrid functional for solids: The HSEsol functional. *J. Chem. Phys.* **2011**, *134*, 024116.
(50) Tran, F.; Stelzl, J.; Blaha, P. Rungs 1 to 4 of DFT Jacob's ladder: Extensive test on the lattice constant, bulk modulus, and cohesive energy of solids. *J. Chem. Phys.* **2016**, *144*, 204120.
(51) Zhang, G.-X.; Reilly, A. M.; Tkatchenko, A.; Scheffler, M. Performance of various density-functional approximations for cohesive properties of 64 bulk solids. *New J. Phys.* **2018**, *20*, 063020.
(52) Saßnick, H. D.; Cocchi, C. Electronic structure of cesium-based photocathode materials from density functional theory: Performance of PBE, SCAN, and HSE06 functionals. *Electron. Struct.* **2021**, *3*, 027001.
(53) Takikawa, Y.; Ebisu, S.; Nagata, S. Van Vleck paramagnetism of the trivalent Eu ions. *J. Phys. Chem. Solids* **2010**, *71*, 1592−1598.
(54) Van Vleck, J. H. *The Theory of Electric and Magnetic Susceptibilities*; Oxford University Press, 1932; pp 245−249.
(55) Anisimov, V. I.; Zaanen, J.; Andersen, O. K. Band theory and Mott insulators: Hubbard *U* instead of Stoner *I*. *Phys. Rev. B: Condens. Matter Mater. Phys.* **1991**, *44*, 943−954.
(56) Cococcioni, M.; De Gironcoli, S. Linear response approach to the calculation of the effective interaction parameters in the LDA+*U* method. *Phys. Rev. B: Condens. Matter Mater. Phys.* **2005**, *71*, 035105.
(57) Richard, D.; Muñoz, E. L.; Rentería, M.; Errico, L. A.; Svane, A.; Christensen, N. *Abinitio* LSDA and LSDA+*U* study of pure and Cd-doped cubic lanthanide sesquioxides. *Phys. Rev. B: Condens. Matter Mater. Phys.* **2013**, *88*, 165206.
(58) Richard, D.; Errico, L. A.; Rentería, M. Structural properties and the pressure-induced C → A phase transition of lanthanide

https://doi.org/10.1021/jacs.3c11615
J. Am. Chem. Soc. 2024, 146, 2113−2121

sesquioxides from DFT and DFT+*U* calculations. *J. Alloys Compd.* **2016**, *664*, 580−589.
(59) Tanner, P. A. Some misconceptions concerning the electronic spectra of tri-positive europium and cerium. *Chem. Soc. Rev.* **2013**, *42*, 5090−5101.
(60) Zakaria, D.; Mahiou, R.; Avignant, D.; Zahir, M. Single-crystal structure refinement and luminescence analysis of β-$NaEuF_4$. *J. Alloys Compd.* **1997**, *257*, 65−68.
(61) Wang, Y.; Lian, Z.; Su, X.; Yang, Z.; Pan, S.; Yan, Q.; Zhang, F. $Cs_6RE_2(PO_4)_4$ (RE = Y and Gd): two new members of the alkali rare-earth double phosphates. *New J. Chem.* **2015**, *39*, 4328−4333.
(62) Tisdale, H. B.; Christian, M. S.; Morrison, G.; Besmann, T. M.; Sun, K.; Was, G. S.; zur Loye, H.-C. Investigation of Rare Earth-Containing Double Phosphates of the Type $A_3Ln(PO_4)_2$ (Ln= Y, La, Pr, Nd, and Sm−Lu) as Potential Nuclear Waste Forms. *Chem. Mater.* **2022**, *34*, 3819−3830.
(63) Essehli, R.; El Bali, B.; Dusek, M.; Fejfarova, K.; Lachkar, M. Yttrium hydrogendiphosphate trihydrate. *Acta Crystallogr., Sect. E: Struct. Rep. Online* **2007**, *63*, i80−i82.
(64) Essehli, R.; Lamhamdi, A.; Alaoui, A. T.; El Bali, B.; Mejdoubi, E.; Lachkar, M.; Dusek, M.; Fejfarova, K. $AErP_2O_7$ (A = Rb, Cs) and $HEuP_2O_7{\cdot}3H_2O$: Crystal Structures, Vibrational Studies and Thermal Behaviours. *J. Chem. Crystallogr.* **2012**, *42*, 475−485.
(65) Mbarek, A. Synthesis, structural and optical properties of Eu^{3+}-doped $ALnP_2O_7$ (A = Cs, Rb, Tl; Ln= Y, Lu, Tm) pyrophosphates phosphors for solid-state lighting. *J. Mol. Struct.* **2017**, *1138*, 149−154.
(66) Zhao, D.; Ma, F.; Zhang, R.; Zhang, R.; Zhang, L.; Fan, Y. Crystal structure and luminescence properties of self-activated phosphor $CsDyP_2O_7$. *Mater. Res. Bull.* **2017**, *87*, 202−207.
(67) Chen, G.; Hölsä, J.; Peterson, J. A luminescence study of single-crystal $EuPO_4$ at high pressure. *J. Phys. Chem. Solids* **1997**, *58*, 2031−2037.
(68) Hamady, A.; Jouini, T. $Na_7Y_2(P_2O_7)_2(P_3O_{10})$ − a new layer and tunnel structure. *Z. Anorg. Allg. Chem.* **1996**, *622*, 1987−1990.
(69) Averbuch-Pouchot, M.; Durif, A. Crystal Chemistry of Oligophosphates. *Annu. Rev. Mater. Sci.* **1991**, *21*, 65−92.
(70) Durif, A. *Crystal Chemistry of Condensed Phosphates*; Springer Science & Business Media, 1995.
(71) Attfield, J. P. *Encyclopedia of Inorganic and Bioinorganic Chemistry*; John Wiley & Sons, Ltd, 2014; pp 1−16.
(72) Barsukov, I. V.; Syt'ko, V. V.; Umreiko, D. S. Influence of the structure of the $MEu(PO_3)_4$ crystals on their luminescent properties. *J. Appl. Spectrosc.* **2004**, *71*, 676−680.
(73) Brecher, C. Europium in the ultraphosphate lattice: Polarized spectra and structure of EuP_5O_{14}. *J. Chem. Phys.* **1974**, *61*, 2297−2315.
(74) Blanzat, B.; Denis, J.-P.; Loriers, J. Luminescence, structural properties and energy transfer mechanisms in some rare earth ultraphosphates. *Proceedings of the Tenth Rare Earth Research Conference*, 1973; pp 1170−1177.
(75) Blanzat, B.; Boehm, L.; Jørgensen, C.; Reisfeld, R.; Spector, N. Transition probabilities of europium (III) in zirconium and beryllium fluoride glasses, phosphate glass, and pentaphosphate crystals. *J. Solid State Chem.* **1980**, *32*, 185−192.
(76) van Vliet, J. P. M.; Blasse, G.; Brixner, L. H. Luminescence properties of the system $Gd_{1-x}Eu_x(IO_3)_3$. *J. Electrochem. Soc.* **1988**, *135*, 1574−1578.
(77) Zhang, X.; Chen, P.; Wang, Z.; Zhou, L.; Zhou, F. Structure and spectroscopic properties of $(Y, Eu)(PO_3)_3$ polyphosphate red phosphors. *Solid State Sci.* **2016**, *58*, 80−85.
(78) Zhu, J.; Cheng, W.-D.; Zhang, H. Caesium europium (III) polyphosphate, $CsEu(PO_3)_4$. *Acta Crystallogr., Sect. E: Struct. Rep. Online* **2009**, *65*, i70.
(79) Zhu, J.; Cheng, W.-D.; Wu, D.-S.; Zhang, H.; Gong, Y.-J.; Tong, H.-N.; Zhao, D. Crystal and band structures, and optical characterizations of sodium rare earth phosphates $NaLnP_2O_7$ and $NaLn(PO_3)_4$ (Ln= Ce, Eu). *J. Alloys Compd.* **2008**, *454*, 419−426.
(80) Sekita, M.; Minami, F.; Okamoto, E.; Masui, H. Optical Spectra of EuP_5O_{14} between 77 and 583 K. *Phys. Status Solidi B* **1980**, *101*, 353−361.
(81) Phanon, D.; Mosset, A.; Gautier-Luneau, I. New iodate materials as potential laser matrices. Preparation and characterisation of α-$M(IO_3)_3$ (M = Y, Dy) and β-$M(IO_3)_3$ (M = Y, Ce, Pr, Nd, Eu, Gd, Tb, Dy, Ho, Er). Structural evolution as a function of the Ln^{3+} cationic radius. *Solid State Sci.* **2007**, *9*, 496−505.
(82) Xu, W.; Xu, H.; Wang, S.; Wang, Z.; Xu, X.; Zhang, X.; Wu, S. Scintillation materials based on metal iodates by rare earth doping modifications for use in radioluminescence and X-ray imaging. *CrystEngComm* **2021**, *23*, 4103−4108.
(83) Ushakov, S. V.; Helean, K. B.; Navrotsky, A.; Boatner, L. A. Thermochemistry of rare-earth orthophosphates. *J. Mater. Res.* **2001**, *16*, 2623−2633.
(84) Cannas, M.; Manca, E.; Pinna, G.; Bettinelli, M.; Speghini, A. Structural investigation of amorphous europium metaphosphate by X-ray diffraction. *Z. Naturforsch., A: Phys. Sci.* **1998**, *53*, 919−927.
(85) Buijs, M.; Blasse, G. One-and three-dimensional energy migration in dimorphic EuP_3O_9. *J. Lumin.* **1988**, *39*, 323−334.
(86) Shelby, R. M.; Macfarlane, R. M. Frequency-dependent optical dephasing in the stoichiometric material EuP_5O_{14}. *Phys. Rev. Lett.* **1980**, *45*, 1098−1101.
(87) Flinn, G. P.; Jang, K. W.; Ganem, J.; Jones, M. L.; Meltzer, R. S.; Macfarlane, R. M. Sample-dependent optical dephasing in bulk crystalline samples of Y_2O_3:Eu^{3+}. *Phys. Rev. B: Condens. Matter Mater. Phys.* **1994**, *49*, 5821−5827.
(88) Sellars, M. J.; Fraval, E.; Longdell, J. J. Investigation of static electric dipole−dipole coupling induced optical inhomogeneous broadening in Eu^{3+}:Y_2SiO_5. *J. Lumin.* **2004**, *107*, 150−154.
(89) Bartholomew, J. G.; Zhang, Z.; Di Lieto, A.; Tonelli, M.; Goldner, P. High resolution spectroscopy of the $^7F_0 \leftrightarrow {}^5D_0$ transition in Eu^{3+}:KYF_4. *J. Lumin.* **2016**, *171*, 221−225.
(90) Casabone, B.; Benedikter, J.; Hümmer, T.; Oehl, F.; Lima, K. d. O.; Hänsch, T. W.; Ferrier, A.; Goldner, P.; Riedmatten, H. d.; Hunger, D. Cavity-enhanced spectroscopy of a few-ion ensemble in Eu^{3+}:Y_2O_3. *New J. Phys.* **2018**, *20*, 095006.
(91) Malinowski, M.; Kaczkan, M. Absorption intensity analysis and emission properties $KEu(PO_3)_4$ and $KEu_xY_{1-x}(PO_3)_4$ crystals. *J. Lumin.* **2019**, *211*, 138−143.

https://doi.org/10.1021/jacs.3c11615
J. Am. Chem. Soc. 2024, 146, 2113−2121